

## Article

# Methyl Orange Adsorption on Biochar Obtained from *Prosopis juliflora* Waste: Thermodynamic and Kinetic Study

Carlos Diaz-Uribe <sup>1</sup>, Jarith Ortiz <sup>1</sup>, Freider Duran <sup>1</sup> , William Vallejo <sup>1,\*</sup>  and Jayson Fals <sup>2</sup>

<sup>1</sup> Grupo de Fotoquímica y Fotobiología, Facultad de Ciencias Básicas, Universidad del Atlántico, Puerto Colombia 81007, Colombia; carlosdiaz@mail.uniatlantico.edu.co (C.D.-U.); jsamuelortiz@mail.uniatlantico.edu.co (J.O.); fgduaran@mail.uniatlantico.edu.co (F.D.)

<sup>2</sup> Grupo de Investigación en Oxi/Hidrotratamiento Catalítico y Nuevos Materiales, Facultad de Ciencias Básicas, Universidad del Atlántico, Puerto Colombia 81007, Colombia; jaysonfals@mail.uniatlantico.edu.co

\* Correspondence: williamvallejo@mail.uniatlantico.edu.co; Tel.: +57-53599484

**Abstract:** In the information contained herein, we fabricated biochar by means of a pyrolysis process; it used *Prosopis juliflora* waste (PJW) as a biomass source. The physical and chemical material characterization was carried out through FTIR, thermogravimetric, BET-N<sub>2</sub> isotherm, and SEM-EDX assays. We studied the methylene orange (MO) adsorption onto PJW biochar. The PJW biochar displayed a maximum percentage of MO removal of 64%. The results of the adsorption study indicated that Temkin isotherm was suitable to describe the MO adsorption process on PJW biochar; it suggests that the MO adsorption on PJW biochar could be a multi-layer adsorption process. Results showed that the pseudo-second-order model was accurate in demonstrating the MO adsorption on PJW ( $k_2 = 0.295 \text{ g mg}^{-1} \text{ min}^{-1}$ ;  $q_e = 8.31 \text{ mg g}^{-1}$ ). Furthermore, the results made known that the MO removal by PJW biochar was endothermic ( $\Delta H = 12.7 \text{ kJ/mol}$ ) and a spontaneous process ( $\Delta G = -0.954 \text{ kJ/mol}$ ). The reusability test disclosed that after four consecutive adsorption/desorption cycles, the PJW biochar reduced its MO removal by only 4.3%.

**Keywords:** environmental remediation; adsorption; biochar; recalcitrant compounds



**Citation:** Diaz-Uribe, C.; Ortiz, J.; Duran, F.; Vallejo, W.; Fals, J. Methyl Orange Adsorption on Biochar Obtained from *Prosopis juliflora* Waste: Thermodynamic and Kinetic Study. *ChemEngineering* **2023**, *7*, 114. <https://doi.org/10.3390/chemengineering7060114>

Academic Editor: Santhana Krishna Kumar Alagarsamy

Received: 6 September 2023

Revised: 29 October 2023

Accepted: 7 November 2023

Published: 1 December 2023



**Copyright:** © 2023 by the authors. Licensee MDPI, Basel, Switzerland. This article is an open access article distributed under the terms and conditions of the Creative Commons Attribution (CC BY) license (<https://creativecommons.org/licenses/by/4.0/>).

## 1. Introduction

Industrial development is responsible for the great deterioration of the aquatic environment by producing high concentrations of recalcitrant compounds (e.g., dyes, chemical solvents, hormones, and pesticides) [1,2]. The textile industry generates more than  $7 \times 10^{11}$  tons of dyes annually, putting flora and human beings in danger [3,4]. These dyes have complex chemical structures (e.g., aromatic rings and various functional groups having  $\pi$ -electrons), which make them more difficult to remove from effluents than natural dyes. In addition, these compounds can bio-accumulate into the environment, and they are toxic to human beings [5,6]. The accumulation of these synthetic dyes in aquatic systems reduces sunlight; they affect plants' growth by increasing the chemical oxygen and biochemical demand [7,8]. According to the chemical structure, the synthetic dyes include several kinds of chemical compounds (e.g., azo, Anthraquinone, benzodifuranone, polycyclic aromatic carbonyl, Indigoid, Xanthere, Phtalein, Polymethine, styryl, phthalocyanines, Quinophthalones, Sulfur, Nitro, and Nitroso dyes) [9]. Among these mentioned compounds, azo dyes are frequently used around the world (e.g., 60% of the world demand); Methyl Orange (MO) belongs to this dye category [10]. Figure 1 shows the chemical structure of MO (it is a sulfonated azo dye). This dye is used in the textile industry and as a pH indicator in the biomedical industry. The sulphonic group is responsible for the high MO solubility in water; in addition, the main drawback of MO is the harm to the environment and human beings [11]. Many strategies have been reported to remove MO from the aquatic environment (e.g., biological treatments [12], oxidation [13], membranes [14], adsorption [15], photocatalytic degradation [16], and coagulation–flocculation [17]). However,

despite different options, the traditional methods have some disadvantages that include energy requirements, costs, incomplete removal, and harmful by-products [18,19].

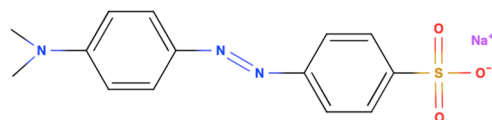


**Figure 1.** Chemical structure of MO.

Among these options, the adsorption method is an attractive removal option due to different advantages (e.g., great efficiency, easy implementation, recyclability, versatility, and smaller cost than other technologies) [20]. Different adsorbents have been reported to remove dyes from various matrices [21]: (i) Activated carbon is a traditional option for MO removal; however, the costs of synthesis and recycling are high [22]. (ii) Bio-sorbents are materials with biological origin (e.g., plant leaves, fish scales, tree bark, and egg shells) that can be transformed to remove different kinds of pollutants from water; they are inexpensive, and they are available. Furthermore, living and dead biomass can be used to remove a number of pollutants [23]. (iii) Nanoparticles of transition metal oxides (e.g., FeO, ZnO, TiO<sub>2</sub>, Cr<sub>2</sub>O<sub>3</sub>, and graphene) are chemically and physically stable and have a great active area for adsorption of different pollutants [24]. (iv) Clays from various sources (e.g., zeolite, kaolinite, goethite, and bentonite) reported great adsorption capacities for dyes, and they are highly valued as adsorbents [25]. (v) Polymers and resins (e.g., polyamide resin, polyamine resin, chitosan, and hydrogels) can be utilized as sorbents in both natural and synthetic forms. The great ease of processing methodology and great versatility of physical forms (e.g., beads and members) are some of the main advantages of polymers as sorbents [26]. (vi) Biochar is a special type of material that has attracted attention in the purification water field. Biochar is considered a potential source of solid energy; in addition, it is suitable for the disposal of agricultural biomass waste [27]. The thermochemical conversion of biomass derived from carbonaceous materials in an oxygen-reduced atmosphere is called biochar [28]. The final properties of biochar depend on the experimental conditions and the method employed to fabricate it. Thermochemical methods can be divided into (i) pyrolysis, (ii) gasification, (iii) liquefaction, and (iv) direct combustion. Among these, pyrolysis stands out as the most cost-effective method because of the versatility of its by-products (e.g., bio-oil, biochar, and syngas) [29]. Traditionally, biochar is utilized to remove toxic metal ions (e.g., Pb<sup>2+</sup> and Cd<sup>2+</sup>) from the water [30–32]. However, In recent decades, biochar has been utilized to remove dyes from the water. Table 1 lists some different adsorbent materials utilized in dye removal from an aqueous solution.

**Table 1.** Adsorbent materials utilized in various dye removal from water.

Material Adsorbent/Reference	Dye	Adsorption Capacity (mg g <sup>-1</sup> )
Chitosan [33]	Indigo carmine	118
Goethite [34]	Methylene orange	55
Zeolite [35]	Crystal violet	1217
Carbonized pine needles [36]	Malachite green	97
Coir pith [37]	Crystal violet	66
MgO–TiO <sub>2</sub> zeolite [38]	Methylene orange	95
Coir pith [37]	Crystal violet	66
Fe–Mn oxide nanoparticles [39]	Methylene blue	72
leaves of populus tree [40]	Methylene orange	90
Orange peel biochar [41]	Congo red	155

The feedstock of biochar can be waste biomasses from plant and/or animal origin. This is a potential opportunity to include sustainability into the agro-industrial process for transforming materials from waste to value-added products. This is a special challenge from the perspective of a circular economy, where recycling and reusing materials is an

important requirement [42]. Currently, studies on the synthesis and practical development removal applications of biochar are a prominent topic of research around the world [43]. Conventionally, natural waste by-products are rejected; nevertheless, they have the potential to transform into biochar [44]. Shalini et al. obtained biochar through agricultural waste as a sustainable alternative to carbon sources to reduce CO<sub>2</sub> emissions [45]. He et al. discussed the advantages of biochar being used in the treatment of municipal wastewater [46]. There are numerous reviews about using biochar from different biomass wastes to develop sustainable applications that verify the importance of biochar production for environmental stability and applications for circular bio-economy [47–49]. A special application of biochar is the removal of dyes from aqueous samples. Sew et al. reported Congo red and crystal violet removal by using biochar obtained from four different sources. They reported that Korean cabbage showed higher adsorption capacity (1304 mg g<sup>-1</sup>) for crystal violet dye [50]. Nithyalakshmi et al. reported the study of dye removal of three different dyes when using biochar obtained from two different sources; in the best case, they reported an efficiency of 87% in the removal of basic fuchsin red from water [51]. Elhamid et al. reported a removal efficiency of 44.6 mg g<sup>-1</sup> for crystal violet dye onto biochar obtained from rice straw waste [52]. Every agricultural country around the world has the potential to become a waste source to produce biochar. Actually, in the Colombian Caribbean region, *Prosopis juliflora* waste (P JW) is widely available, affordable in cost, and can grow in arid climates. *Prosopis juliflora* plants are located in the tropical dry forest region of the department of Atlántico in Colombia. This plant is grown in the backyards of the local houses to reduce internal temperatures. During the first quarter of the year, these plants begin the production of their seeds, which become wastes that are subsequently burned, and this causes problems of environmental pollution, or the wastes are eliminated as solid waste in the garbage [53]. The P JW bioaccumulates and becomes a risk to the region because P JW can contribute to the transmission capacity of parasitic diseases [54]. The P JW is rich in cellulose and lignin. These compounds can be used to prepare activated carbons by pyrolysis [55]. The P JW has demonstrated its potential as biochar. In a previous report, we studied the removal efficiency of methylene blue from an aqueous solution using biochar produced from P JW. In that report, P JW was able to remove 69% of methylene dye from water [56].

In this work, we used P JW as a source of biochar to remove MO from an aqueous solution.

## 2. Materials and Methods

### 2.1. Synthesis and Characterization of Biochar

First, P JW was collected at Piojó (Atlántico–Colombia). Next, the sample was washed and dried at 105 °C. Then, the clean biomass was milled and put in a pyrolysis reactor. After that, the pyrolysis was performed using a heat rate of 5 °C/min until it reached 500 °C. Finally, the sample was espoused at 500 °C for 2 h [57]. The physical–chemical properties of the sorbent were determined through scanning electron microscopy (an Quanta FEG 650 microscope, Brand FEI, Oregon, USA was used), Fourier Transform Infrared spectroscopy (ECO-ATR α—FTIR spectrometer, Brand Bruker, MA, USA), and Differential Scanning Calorimetry analysis (a TGA 5500-Discovery analyzer, Brand TA Instruments, New Castle, USA was used).

### 2.2. Kinetic and Thermodynamic Study

We used two different concentrations of MO (20 ppm and 150 ppm) to study MO removal on P JW biochar (Volume = 25 mL, pH = 6.0, and temperature of 298 K). For each test, we utilized 0.100 g of P JW biochar. The MO concentration was determined by spectrophotometry at 464 nm (MO calibration curve, R = 0.997). We studied the effect of pH and ion strength on the MO removal efficiency. The pH value was changed between 6.0 and 11.0, and the ion strength was changed by a salt addition method by adding KCl in the adsorption system [58].

In the kinetic study, we obtained the MO adsorption capacity on PJW biochar according to the following:

$$q_t = \frac{((C_0 - C_t) \cdot V)}{m} \quad (1)$$

where  $C_t$  (mg/L) is the MO concentration in the solution as a function of time. To model kinetic results, we utilized the pseudo-first-order (2) [59]:

$$\ln(q_t - q_e) = \ln(q_e) - k_1 t \quad (2)$$

where  $q_t$  is the MO amount of anchored per unit mass of the adsorbent ( $\text{mg g}^{-1}$ ) every time.  $q_e$  is the maximum sorption capacity ( $\text{mg g}^{-1}$ ) and  $k_1$  ( $\text{min}^{-1}$ ) is the rate constant. We also applied pseudo-second-order (3):

$$\frac{t}{q_t} = \frac{1}{k_2 q_e^2} + \frac{t}{q_e} \quad (3)$$

where  $k_2$  ( $\text{g mg}^{-1} \text{min}^{-1}$ ) is the rate constant. Finally, we utilized the intraparticle diffusion model (4):

$$q_t = k_{id} t^{1/2} + C \quad (4)$$

where the  $k_{id}$  ( $\text{mg/g}^{-1} \text{min}^{1/2}$ ) is the intraparticle diffusion rate constant.

In the isothermal study, we determined the adsorption capacity of MO on the PJW biochar according to the following:

$$q_e = \frac{V(C_0 - C_e)}{m} \quad (5)$$

where  $q_e$  is the amount (mg) of MO adsorbed per gram of biochar (mg/g) at equilibrium;  $C_0$  is the initial MO concentration (mg/L);  $C_e$  is the MO concentration at equilibrium;  $V$  (L) is the volume of the system; and  $m$  (g) is the amount of biochar. Adsorption data were fit to the Freundlich, Langmuir, and Temkin isotherm models. The Langmuir isotherm model according to the following [60]:

$$\frac{C_e}{q_e} = \frac{1}{K_L q_m} + \frac{C_e}{q_m} \quad (6)$$

where  $q_e$  (mg/g) is the MO amount (mg) adsorbed on biomass (g) at equilibrium condition;  $q_m$  is the Langmuir maximum uptake of MO per gram of biomass (mg/g);  $K_L$  (L/mg) is the Langmuir constant. We applied the Freundlich isotherm model [61]:

$$\ln q_e = \ln K_F + \frac{1}{n} \ln C_e \quad (7)$$

$K_F$  ( $(\text{mg/g})(\text{L/mg})^{1/n}$ ) and  $n$  are Freundlich constants, and  $C_e$  (mg/L) is the equilibrium concentration of MO. Finally, we applied the Temkin isothermal model [62]:

$$q_e = \frac{RT}{b_T} \ln A_T + \frac{RT}{b_T} \ln C_e \quad (8)$$

where  $b_T$  is the Temkin constant, which is related to the heat of sorption (J/mol),  $A_T$  is the equilibrium binding constant (L/mg),  $T$  is the absolute temperature, and  $R$  is the gas constant. The fitting correlation coefficient ( $R^2$ ) and an average relative error (ARE) were used to determine the best-fitting isotherm:

$$ARE = \frac{100}{n} \sum_{i=1}^n \frac{|q_e - q_f|}{q_e} \quad (9)$$

where  $q_e$  is the experimental value,  $q_f$  is the fitted value, and  $n$  is the number of data points. Finally, we calculated the thermodynamic parameters of the adsorption process, Gibbs free energy ( $\Delta G^0$ ), enthalpy ( $\Delta H^0$ ), and entropy ( $\Delta S^0$ ) according to the following:

$$K = \frac{q_e}{C_e} \quad (10)$$

$$\Delta G^0 = -RT \ln K \quad (11)$$

$$\ln K = \frac{\Delta S^0}{R} - \frac{\Delta H^0}{RT} \quad (12)$$

Here,  $T$  is the absolute temperature (K);  $R$  is the universal gas constant ( $8.314 \text{ J mol}^{-1}\text{K}^{-1}$ ); and  $K$  is the thermodynamic equilibrium constant.

### 3. Results and Discussion

#### 3.1. PJW-Biochar Characterization

The FTIR spectrum of PJW biochar is shown in Figure 2. The broad band located between  $2850$  and  $2750 \text{ cm}^{-1}$  corresponds to C-H stretching ( $\text{sp}^2$ ) and C-H stretching ( $\text{sp}^3$ ), respectively. The broad band located between  $2428$  and  $2314 \text{ cm}^{-1}$  is related to deformation vibrations in the  $\text{C}\equiv\text{C}$  plane [63]. This is an important chemical group because the MO molecule can interact through electrostatic  $\pi$ - $\pi$  interaction to anchor to the biochar surface. This band appears in the FTIR spectrum of the biochar derived from maize straw [64]. The bands located near  $1650$  and  $1460 \text{ cm}^{-1}$  are assigned to C=C stretch and C-C inside of the aromatic ring. At the region of  $1002 \text{ cm}^{-1}$ , the strong band is assigned to the C-O stretching vibration in cellulose and hemicellulose [65,66]. Furthermore, it is related to materials with a high content of cellulose and lignin, which confirms the major constituent PJW biochar [67]. After MO adsorption on the biochar surface, the main signals are conserved. Although a broad band appears located between  $3500$  and  $3000 \text{ cm}^{-1}$ , this band corresponds to the -OH bond [68]. The signal located at  $1002 \text{ cm}^{-1}$  reduces its intensity due to the MO adsorption and the surface covering. The broad band located between  $1670$  and  $1511 \text{ cm}^{-1}$  is shifted in comparison with the biochar spectrum; this shifting and broadening are attributed to the MO anchoring, and this band can overlap the corresponding peaks to the C-H bending of aromatic rings (peaks located at  $1676 \text{ cm}^{-1}$  and  $1646 \text{ cm}^{-1}$ ). In addition, -N=N- stretching vibrations (peaks located at  $1600 \text{ cm}^{-1}$  and  $1516 \text{ cm}^{-1}$ ) corresponds to the MO molecule [69].

Figure 3 shows the BET isotherms of  $\text{N}_2(\text{g})$  onto PJW biochar. Results demonstrate a typical behavior that relates to isotherm type II. This behavior is associated with porous solids with a crack-like shape. The BET surface area was  $1.28 \text{ m}^2\text{g}^{-1}$ , and the pore size was  $26 \text{ nm}$ , with a pore volume of  $1.14 \times 10^{-4} \text{ cm}^3/\text{g}$ . These results are comparable with other previous reports about other biochars. Pawar et al. reported a surface area of  $0.987 \text{ m}^2\text{g}^{-1}$  for a biochar obtained from *P. juliflora* [70], and Selvarajoo et al. reported a surface area of  $0.272 \text{ m}^2\text{g}^{-1}$  for a biochar obtained from palm fiber [71]. Stylianou et al. reported a surface area of  $1.53 \text{ m}^2\text{g}^{-1}$  for a biochar obtained from spent coffee grounds [72]. Antonangelo et al. reported a surface area of  $1.0 \text{ m}^2\text{g}^{-1}$  for a biochar derived from switchgrass [73]. However, the BET area was smaller than other biochar reports:  $8 \text{ m}^2\text{g}^{-1}$  for biochar obtained from straw [74] and  $372 \text{ m}^2\text{g}^{-1}$  for biochar obtained from Miscanthus [75]. In spite of the small BET area of PJW, this chemical modification is a sustainable option to utilize agricultural waste. It is an opportunity to generate value added to the agriculture waste.

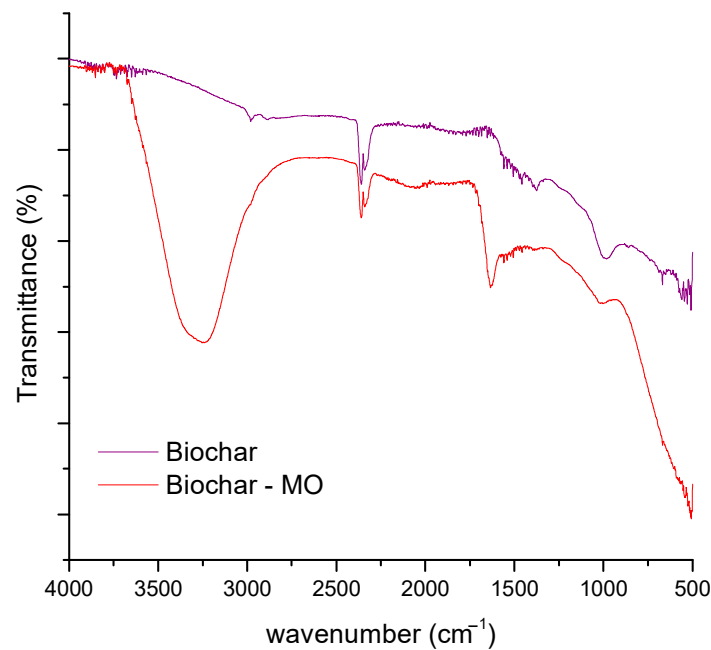


**Figure 2.** Fourier Transform Infrared spectrum of the PJW biochar.

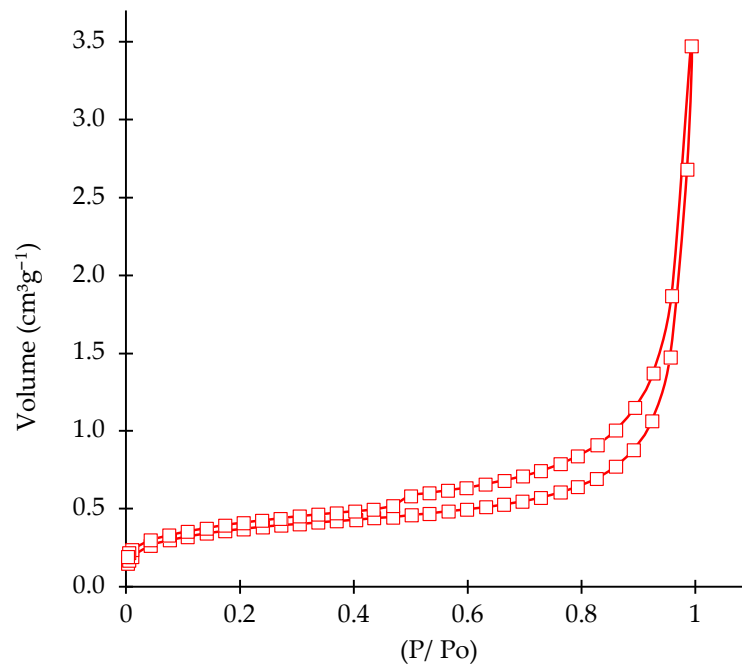


**Figure 3.** BET  $N_{2(g)}$  isotherm adsorption onto PJW biochar.

The results for the thermal characterization of PJW are shown in Figure 4. Results exhibit the thermogravimetric thermograph, and Table 2 lists the data and the assignment for each loss of weight. During pyrolysis, the basic components of biomass (e.g., lignin and cellulose) degraded between 250 and 600 °C; according to Figure 4, this process occurs between 420 and 570 °C with a loss of weight of 68%. This result is according to a material with a high content of cellulose and lignin [70,71]. The final composition of biochar is affected by (i) the type of feedstock material utilized as a biochar source, (ii) the pyrolysis condition (temperature and temperature ramp), and (iii) modification approaches. The DSC curve for PJW biochar is shown in Figure 4b. Results show an endothermic peak; this signal is associated with the typical endothermic melting of biochar at 139 °C.

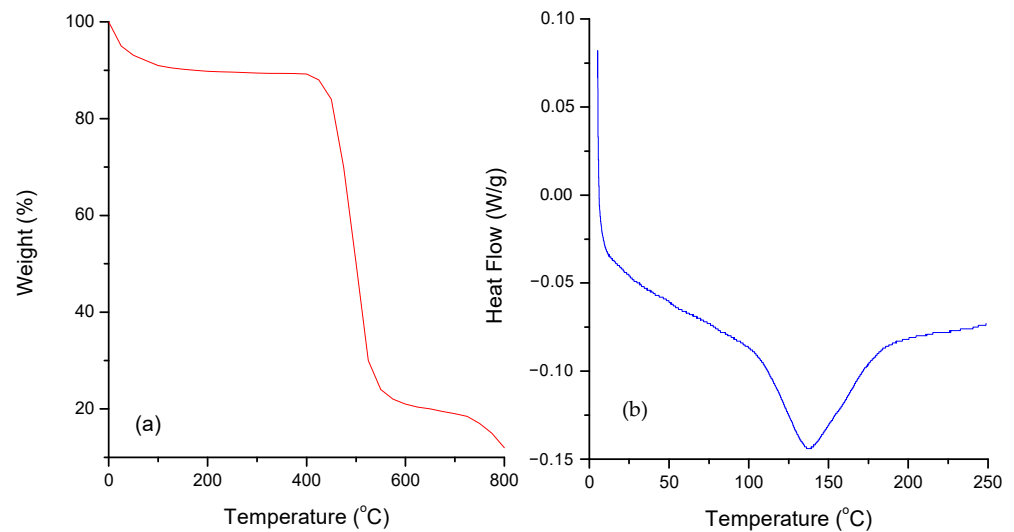


**Figure 4.** (a) TGA thermograph of PJW biochar. (b) DSC thermograph curve for PJW biochar.

**Table 2.** Thermogravimetric results.

Temperature (°C)	Loss (%) <sup>1</sup>	Assignment
20–50	5	H <sub>2</sub> O volatile organic solvent
420–570	68	Cellulose degradation and lignin oxidation
570–800	10	Carbonization

<sup>1</sup> Data obtained from Figure 3a.

Figure 5 shows the SEM images for PJW biochar. Results show that the PJW surface morphology was heterogeneous and structurally complex. Results show a mesoporous and rough texture. These cavities are large enough to allow the diffusion of MO (the MO molecular diameter is estimated to be about 6–8 nm) [76]. The porosity is associated with the freeing of small molecules (e.g., water, methane, and carbon dioxide) throughout the synthesis process and the losses of lignin and cellulosic derivatives during pyrolysis [72]. Additionally, Figure 6 shows the EDX spectrum of PJW biochar. This figure shows PJW biochar was composed mainly of carbon, oxygen, and other remaining elements (e.g., Mg, K, Ca, and P). The EDX assay was carried out in three areas on the surface, and Table 3 lists the average composition results. The adsorption properties are affected by the composition of feedstock due to the presence of minerals that can contribute to the formation of the additional active site on biochar to improve its potential removal capacity.

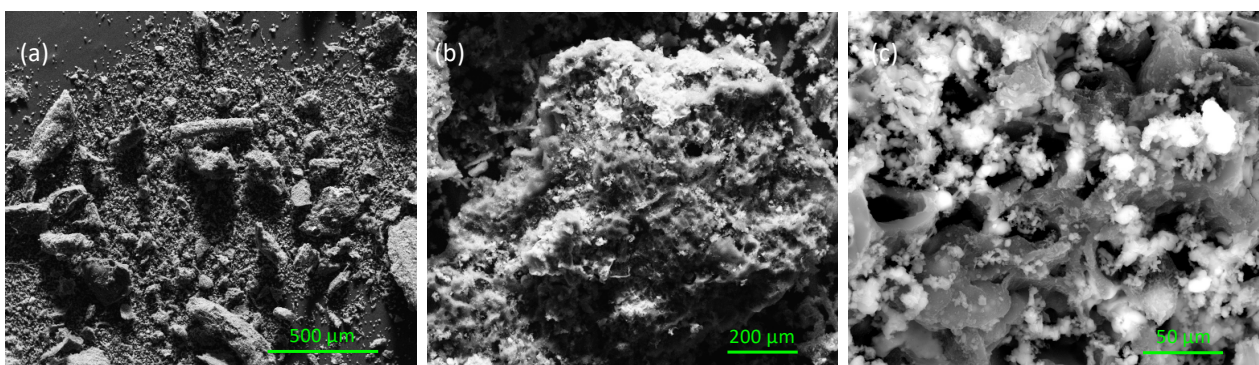


**Figure 5.** SEM images of PJW were obtained in this work with different magnifications: (a) ×100, (b) ×600, and (c) ×6000.

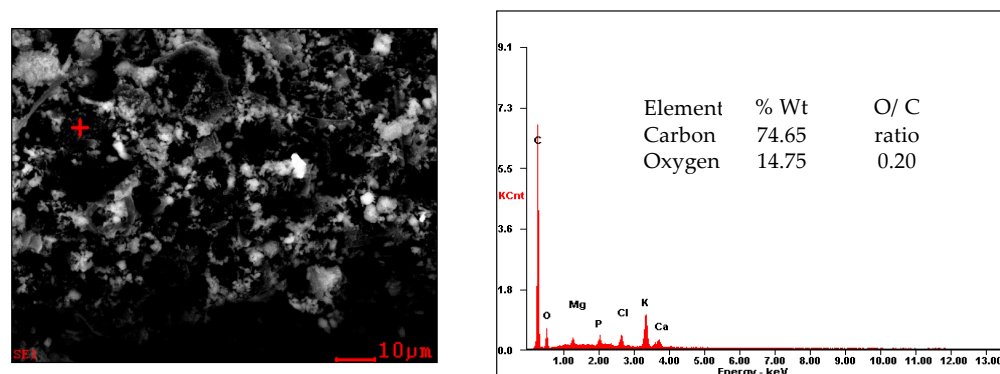


Figure 6. EDX spectrum of zone 1 on the PJW biochar surface.

Table 3. Content of elements of the PJW biochar.

Element Line	Area 1 (wt.%) <sup>1</sup>	Area 2 (wt.%) <sup>1</sup>	Area 3 (wt.%) <sup>1</sup>	Average (wt.%) <sup>1</sup>
C K	74.65	64.81	69.22	69.56
O K	14.75	14.19	13.50	14.14
Mg K	1.15	1.32	0.42	0.96
P K	1.03	1.72	--	--
K K	5.25	11.91	9.52	8.89
Ca K	1.39	1.72	--	--
Cl K	1.77	5.12	5.94	4.27
Mo L	--	--	1.25	--

<sup>1</sup> Data obtained from EDX assay.

EDX results (Table 3) show that PJW biochar was composed mainly of carbon (69.56%) and oxygen (14.14%). After the pyrolysis process, the resulting biochar was rich in carbon elements; this is an important aspect because this material can be suitable for removing organic and inorganic pollutants from water [77]. Among the remaining elements, potassium was in the highest ratio. The presence of those ions needs to be monitored carefully. A high potassium ion concentration element is associated with agglomeration problems; in our case, K content was (7%). Other authors reported that those inorganic components can affect the gasification reactivity [71].

### 3.2. Kinetic Study of MO Adsorption on PJW Biochar

Two different concentrations of MO (20 ppm and 150 ppm) were used to study the MO concentration impact on the removal efficiency. Figure 7 shows the impact of concentrations of MO on the removal percentage. Figure 7 shows the MO removal efficiency was increased as contact time was increasing. Results show the saturation time of the surface was reached after 15 min. Moreover, when the initial MO concentration was increased, the MO removal was reduced; this behavior can be associated with the overload of the available sites for dye anchoring on the PJW surface. Similar behaviors have been reported to Cd adsorption on biochar [59,78]. Figure 8a shows the effect of pH solution on MO removal using PJW. Since the pH value of the solution can affect the charge of the biochar surface, the solution pH value is one of the most important parameters that affect the removal capacity of the biochar. The best removal percentage was obtained at pH = 6.0. Figure 8a shows that at pH values higher than 6.0, the removal efficiency decreases significantly near 0.38% at pH = 11.0. At pH higher than 4.4, the stable chemical structure of MO corresponds to the structure shown in Figure 1. The MO is a typical anionic azo dye; thus, the MO sorption will be favored if the charge of the biochar surface is positive. However, results indicate that as the pH value increases, the MO removal efficiency decreases, indicating that the pH of the surface becomes more negative as pH increases. Van-Phuc reported a pH solution of 5.5 as the optimal in the removal of Pb<sup>2+</sup> and Cd<sup>2+</sup> onto biochar obtained from pomelo

fruit peels. They reported the same tendency in the removal efficiency as a function of the pH [79].

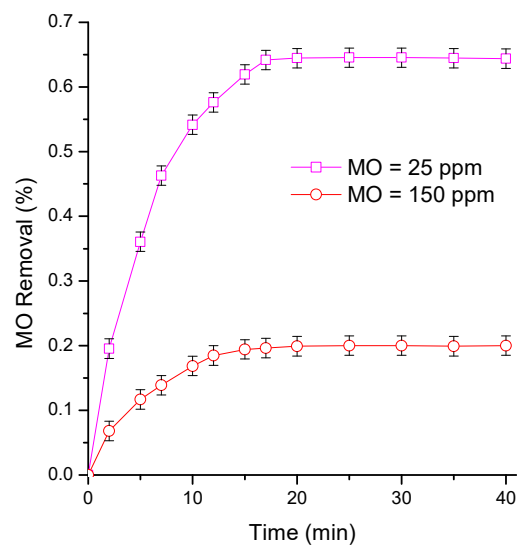


**Figure 7.** Removal efficiency vs. time for different initial concentrations of MO on PJW biochar ( $C_0 = 10$  mg/L, PJW dosage = 0.1 g; stirring rate = 150 rpm, temperature = 298 K, pH = 6.0, error bar = SD, and  $n = 3$ ).

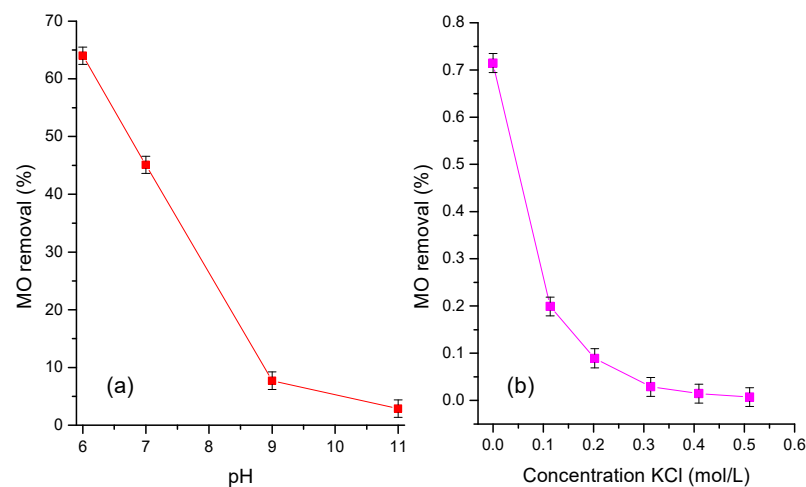


**Figure 8.** Effect of (a) pH solution and (b) ionic strength on the MO removal efficiency on PJW biochar ( $C_0 = 10$  mg/L, PJW dosage = 0.1 g; stirring rate = 150 rpm, temperature = 298 K, error bar = SD, and  $n = 3$ ).

The ionic strength is another parameter of the MO removal efficiency of the biochar since it affects the electrostatic interaction between the biochar surface and the adsorption ions. Figure 8b shows the effect of ionic strength on the MO removal of PJW biochar. The plot indicates removal efficiency decreases as the KCl concentration increases. It is known that electrostatic interactions may also be reduced by increasing the ionic strength of the solution; this behavior is a consequence of the electrostatic screening. As the KCl concentration increases, the electrostatic screening increases, and the charge makes it more difficult for charged particles to be adhered to the surface [80].

We used three kinetic models to study the kinetic mechanism of MO adsorption onto the biochar surface (Equations (2)–(4)). Figure 9 shows the kinetic fitting results, and Table 4 lists the parameters for each model. The mechanism of MO adsorption on biochar can include physical and chemical processes [21].

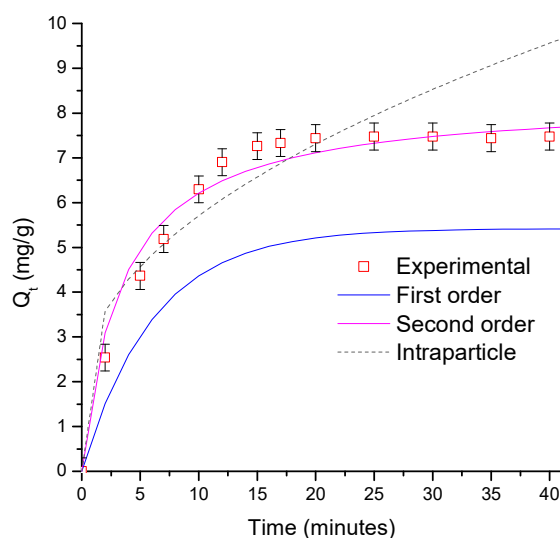


**Figure 9.** Kinetic fitting of MO on PJW biochar (PJW dosage = 0.1 g; stirring rate = 150 rpm, temperature = 298 K, error bar = SD, and  $n = 3$ ).

**Table 4.** Results of kinetic modeling of MO adsorption on PJW biochar.

Fitting Model		Kinetic Values <sup>1</sup>		
Pseudo-first order	$q_e$ (mg g <sup>-1</sup> )	$k_1$ (min <sup>-1</sup> )	$R^2$	ARE (%)
	5.41	0.163	0.914	21.3
Pseudo-second order	$q_e$ (mg g <sup>-1</sup> )	$k_2$ (g mg <sup>-1</sup> min <sup>-1</sup> )		
	8.31	0.295	0.994	4.4
Intraparticle diffusion	$C$ (mg g <sup>-1</sup> )	$k_{id}$ (g mg <sup>-1</sup> min <sup>-1</sup> )		
	1.86	1.22	0.841	10.8

<sup>1</sup> Data obtained from fitting of kinetic models.

The intraparticle diffusion fitting showed the worst fitting results; Figure S1 shows the linear fitting for experimental data. The total data reveal an  $R^2 = 0.841$ ; however, two different regions are distinguished; they suggest the MO adsorption on PJW is not only under intra-particle diffusion but under the control of different mechanisms (e.g., external diffusion and adsorption onto active sites) [81]. Taking into account the PJW pore size (26 nm, Section 3.1) and the estimated value of the molecular diameter of MO (about 6–8 nm [76]), the intra-particle diffusion process could be present during the adsorption process. Nonetheless, the multilinearity of results in Figure S1 indicates that several stages can be available because they determine the kinetics of the adsorption process. Both regions of the plot (Figure S1) must be analyzed independently. The interpretation of these regions is confusing due to different authors responding differently to this phenomenon [82]. Gulliapi et al. attributed the initial part of the curve to the diffusion in the micropores during the adsorption of selenium through rice husk ash. They reported the diffusion in the meso- and micropores represented by the bi-linear in the intraparticle fitting (Figure S1) [83]. In the study of biosorption of methylene blue using *Paspalum notatum*, Kumar et al. explained this region as part of the diffusion in the limit layer [84]. Wang et al. hypothesized that the intraparticle diffusion model occurs in the first part of the model (see black line Figure S1), and the equilibrium of intraparticle diffusion in pores is achieved when both lines are matched. According to Wang et al., if the fitting line (black line Figure S1) passes through the origin point (0, 0), the adsorption is dominated by the intra-particle diffusion; if not, it is a multiple adsorption process [85]. In our case, the fitting line of the first section of the model did not pass exactly through the origin point (0, 0). Thus, intraparticle diffusion is not the only speed-limiting step of the process.

Among kinetic models, the pseudo-second-order (PSO) model showed the best-fitting results. Kinetic results and the ionic strength study suggest that electrostatic interaction

between MO and biochar surface could be an important interaction during the adsorption process. Qiu et al. suggested that pyrolysis temperature  $>400$  °C can lead to an increase in the electrostatic interaction of the biochar [86]. The PSO model has been reported as best-fitting for the removal of various pollutants on biochar previously [87]. Ghani et al. reported that during the pyrolysis process with temperatures lower than 500 °C, the lignin is not converted into a hydrophobic hydrocarbon, and biochar becomes more hydrophilic [88]. Due to the presence of a dye sulphonic group, the MO dye will anchor easily on a hydrophilic surface. The adsorption of methylene blue on PJW biochar reported  $q_e = 2.94$  mg/g and  $k_2 = 0.0867$  [56]; in our case, both of them ( $q_e$  and  $k_2$ ) were greater evidence that PJW biochar is better in the removal of anionic (MO) dye than cationic dye methylene blue.

### 3.3. Isothermal Study of MO Adsorption on PJW Biochar

Figure 10 shows the results of the isothermal study of MO adsorption on PJW biochar. Table 5 lists the physical–chemical parameters. Adsorption data show an L shape, which indicates there is no competition between molecules of water and MO to fill the available sites on the PJW biochar surface [89]. The Temkin and Langmuir models showed the best-fitting results. The Temkin model assumes the adsorption enthalpy is reduced as the adsorption coverage rises and the anchoring energy is dispersed over the anchoring site; this is according to multi-layer adsorption on the heterogeneous biochar [76,90]. Among isothermal models, the Temkin model has the best-fitting values since it suggests MO adsorption on PJW biochar is a multi-layer process that is suitable for the characterization results (Section 3.1). However, if it is compared with other reports (see Table 6), most of them reported that the Langmuir isotherm is the best-fitting model. The Langmuir isotherm assumes a dynamic equilibrium between the rates of sorption/desorption of dye on the biochar surface [91]. In our case, PJW biochar shows a heterogeneous surface according to a multi-layer process. In this case, it is possible that more than one model fits the experimental data because they state that several adsorption processes occur during dye anchoring. The mechanism of MO adsorption on biochar can be explained by various processes (e.g., ion exchange, electrostatic interaction, and pore filling and precipitation). The sulphonic group can interact easily with oxygen that contains groups located on the surface of biochar, and the rest of the MO molecule can interact through an electrostatic  $\pi$ - $\pi$  interaction to anchor to the surface [92]. During the MO adsorption process onto PJW biochar, multiple steps could be present: (i) external mass transfer, (ii) intraparticle diffusion, and (iii)  $\pi$ - $\pi$  interaction and electrostatics interactions [93]. Figure S3 shows a diagram of the process.

Wu et al. studied MO adsorption onto halloysite nanotubes and chrysotile nanotubes, and they reported that the Temkin model was suitable to describe the adsorption process [76]. Comparing the  $q_{\max} = 8.08$  mg/g obtained for PJW biochar with typical reports for active carbon, clays, and nanoparticles of composites, the value reported herein is small. However, the biochar adsorbents obtained from waste contribute to reducing the bio-accumulate process in the environment [44] and offer an alternative for carbon storage [94].

**Table 5.** Results of isothermal modeling of MO adsorption on PJW biochar.

Isothermal Model		Parameters <sup>1</sup>		
Langmuir	$q_{\max}$ (mg g <sup>-1</sup> ) 8.08	$k_L$ (L·min <sup>-1</sup> ) 0.0731	$R^2$ 0.995	ARE (%) 5.4
Langmuir	$K_F$ (mg g <sup>-1</sup> )(L g <sup>-1</sup> ) <sup>1/n</sup> 1.45	$1/n$ 0.368	0.981	8.3
Temkin	$B_T$ 1.52	$A_T$ (L min <sup>-1</sup> ) 1.14	0.999	1.1

<sup>1</sup> Data obtained from fitting of isothermal models.

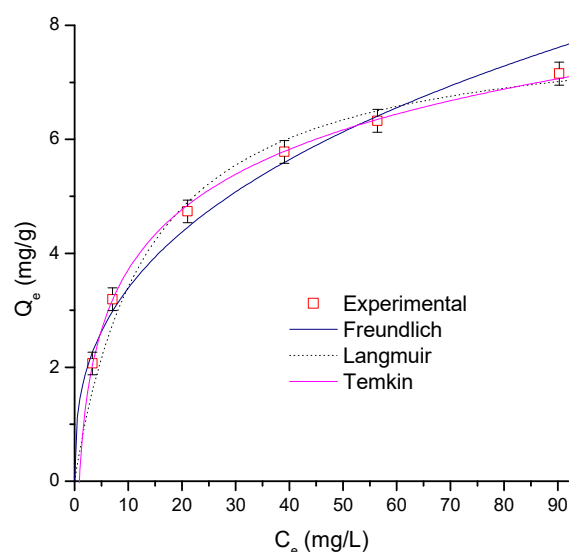


**Figure 10.** Fitting results for isothermal adsorption of MO on PJW biochar (PJW dosage = 0.1 g; stirring rate = 150 rpm, temperature = 298 K, error bar = SD, and n = 3).

### 3.4. Thermodynamic Study

We determined the temperature effect on the MO adsorption process in four temperatures (30, 40, 50, and 60 °C). The thermodynamic parameters were determined from the linear fitting of the Arrhenius equation (Equation (12)). Figure S2 shows the linear fitting plot, and Table 6 lists fitting results for PJW biochar and other adsorbent materials. Table 6 shows the MO adsorption process is thermodynamic spontaneous ( $\Delta G = -0.954$  kJ/mol) on PJW. Also, the reduction in  $\Delta G$  at higher temperatures verifies that the adsorption process is thermodynamically allowed at higher temperatures. On top of that, MO adsorption was an endothermic type process ( $\Delta H = 12.7$  kJ/mol). Comparing the results of PJW with other thermodynamic reports for MO removal from water, they are comparable (see Table 6). The value of  $\Delta G$  was negative for all reports listed, and most of the sorbents reported in Table 6 show positive enthalpy adsorption values related to the endothermic process.

**Table 6.** Thermodynamic properties for MO removal on various adsorbent materials.

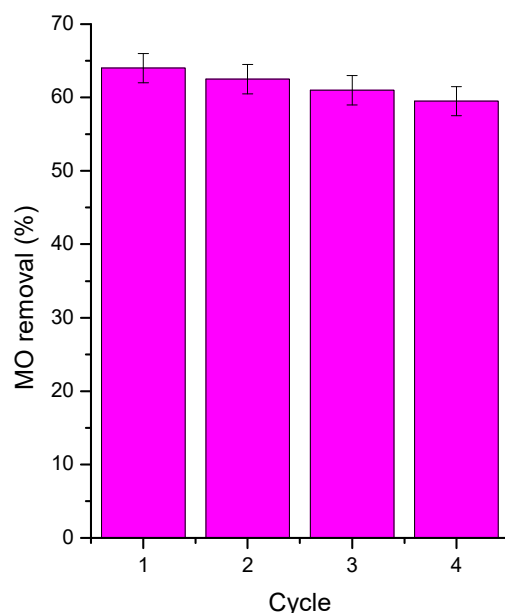
Adsorbent Materials	Isotherm Model	Temperature (K)	Thermodynamic Parameters <sup>1</sup>		
			$\Delta G$ (kJ/mol)	$\Delta H$ (kJ/mol)	$\Delta S$ (J/molK)
PJW	Temkin	303	-0.954	12.7	45.2
		313	-1.406		
		323	-1.859		
		333	-2.311		
Active carbon— <i>Vitis vinifera</i> L. [95]	Freundlich	288	-0.17	39.1	133
		303	-1.91		
		318	-3.13		
CuO [96]	Langmuir	303	-0.256	15.8	58
		318	-1.07		
		333	-1.89		
Modified silkworm exuviae [97]	Langmuir	303	-3.37	2.54	20
		313	-3.54		
		323	-3.78		
PVP-ZnO composite [98]	---	298	-51.2	49.9	171
		308	-52.9		
		318	-54.6		
		298	-51.2		

Table 6. Cont.

Adsorbent Materials	Isotherm Model	Temperature (K)	Thermodynamic Parameters <sup>1</sup>		
			$\Delta G$ (kJ/mol)	$\Delta H$ (kJ/mol)	$\Delta S$ (J/molK)
Orange peels [99]	Langmuir	303	−9.19	49.3	256
		313	−11.3		
		323	−13.5		
		303	−9.19		
Orange peels [100]	Langmuir	298	−25.8	−23.1	9.1
		313	−25.9		
		333	−26.2		
Sugar scum powder [101]	Langmuir	293	−14.6	−14.14	2.03
		303	−14.9		
		318	−14.7		
Chicken manure biochar [102]	Langmuir	303	−2.24	7.56	32.9
		313	−2.63		
		323	−2.90		

<sup>1</sup> Data obtained from Arrhenius equation fitting.

The reusability of biochar is a critical property for industrial applications. The adsorbent stability can be tested under different experimental conditions to determine its impact on the removal capacity of biochar (pressure, temperature, acid and alkali medium, and recyclability) [103]. Figure 11 shows the recyclability capability of PJW biochar after four sorption/desorption cycles. Results showed that after four consecutive cycles, the removal capacity of PJW biochar was reduced by only 4.3%. This suggests that PJW biochar is suitable for removing MO from the water after repetitive cycles. This is an important aspect to include sustainability in the physical transformation process; the biomass waste problem is solved after the biochar production, and the biochar can be used in various cycles to remove a dye from water.



**Figure 11.** Reusability of PJW biochar after 4 sorption/desorption cycles (PJW dosage = 0.1 g; stirring rate = 150 rpm, temperature = 298 K, error bar = SD, and n = 3).

Finally, the PJW is an attractive option to be used as an inexpensive and sustainable biochar source to remove MO from the water.

#### 4. Conclusions

We obtained biochar using PJW as a source of carbonaceous material. The material was heterogeneous and structurally complex. PJW shows a rough texture with a pore size of 26 nm. The FTIR results were suitable with a biochar obtained from a biomass with a high lignin and cellulose content. The PJW biochar displayed a maximum percentage of MO removal of 64%. The pH study showed the removal efficiency was reduced as pH was increased, and besides the ionic strength, results indicated that the electrostatic screening could be presented. The PSO model was suitable to describe the MO adsorption process ( $k_2 = 0.295 \text{ g mg}^{-1} \text{ min}^{-1}$ ;  $q_e = 8.31 \text{ mg g}^{-1}$ ). The thermodynamic results showed the MO removal by PJW biochar was a spontaneous process ( $\Delta G = -0.954 \text{ kJ/mol}$ ) and endothermic type process ( $\Delta H = 12.7 \text{ kJ/mol}$ ). The reusability test indicated that PJW biochar was stable after four consecutive adsorption/desorption cycles. Finally, all the results indicated the PJW is an attractive option to be used as an inexpensive and sustainable biochar source to remove MO from the water.

**Supplementary Materials:** The following supporting information can be downloaded at <https://www.mdpi.com/article/10.3390/chemengineering7060114/s1>. Table S1. List symbols & abbreviations. Figure S1. Intra-particle diffusion fitting for experimental data of MO adsorption on PJW biochar; Figure S2. Linear fitting of Arrhenius equation for MO adsorption on PJW biochar. Figure S3. Possible diagram for MO sorption onto PJW biochar.

**Author Contributions:** Conceptualization, C.D.-U. and W.V.; methodology, C.D.-U., F.D. and W.V.; validation, C.D.-U., J.O., F.D. and W.V.; formal analysis, C.D.-U., J.O., F.D., W.V. and J.F.; investigation, W.V., C.D.-U. and F.D.; resources, W.V., C.D.-U. and F.D.; data curation, C.D.-U., J.O., F.D., W.V. and J.F.; writing—original draft preparation, C.D.-U., J.O., F.D., W.V. and J.F.; writing—review and editing, C.D.-U., J.O., F.D., W.V. and J.F.; visualization, C.D.-U., J.O., F.D., W.V. and J.F.; supervision, W.V. and C.D.-U.; project administration, W.V. and C.D.-U.; funding acquisition, W.V. and C.D.-U. All authors have read and agreed to the published version of the manuscript.

**Funding:** This research was funded by Universidad del Atlántico.

**Data Availability Statement:** Data are contained within the article.

**Conflicts of Interest:** The authors declare no conflict of interest.

#### References

1. Rohani, M.F. Pesticides toxicity in fish: Histopathological and hemato-biochemical aspects—A review. *Emerg. Contam.* **2023**, *9*, 100234. [[CrossRef](#)]
2. Häder, D.P.; Banaszak, A.T.; Villafaña, V.E.; Narvarte, M.A.; González, R.A.; Helbling, E.W. Anthropogenic pollution of aquatic ecosystems: Emerging problems with global implications. *Sci. Total Environ.* **2020**, *713*, 136586. [[CrossRef](#)] [[PubMed](#)]
3. Lellis, B.; Fávoro-Polonio, C.Z.; Pamphile, J.A.; Polonio, J.C. Effects of textile dyes on health and the environment and bioremediation potential of living organisms. *Biotechnol. Res. Innov.* **2019**, *3*, 275–290. [[CrossRef](#)]
4. Muthu, S.S. Evaluation of Sustainability in Textile Industry. In *Sustainability in Textile Industry*; Springer: Singapore, 2017; pp. 9–15.
5. Marrakchi, F.; Ahmed, M.J.; Khanday, W.A.; Asif, M.; Hameed, B.H. Mesoporous-activated carbon prepared from chitosan flakes via single-step sodium hydroxide activation for the adsorption of methylene blue. *Int. J. Biol. Macromol.* **2017**, *98*, 233–239. [[CrossRef](#)] [[PubMed](#)]
6. Guarán, J.R.; Moreno-Pirajan, J.C.; Giraldo, L. Kinetic Study of the Bioadsorption of Methylene Blue on the Surface of the Biomass Obtained from the Algae *D. antarctica*. *J. Chem.* **2018**, *2018*, 2124845. [[CrossRef](#)]
7. Katheresan, V.; Kansedo, J.; Lau, S.Y. Efficiency of various recent wastewater dye removal methods: A review. *J. Environ. Chem. Eng.* **2018**, *6*, 4676–4697. [[CrossRef](#)]
8. Tebeje, A.; Worku, Z.; Nkambule, T.T.I.; Fito, J. Adsorption of chemical oxygen demand from textile industrial wastewater through locally prepared bentonite adsorbent. *Int. J. Environ. Sci. Technol.* **2022**, *19*, 1893–1906. [[CrossRef](#)]
9. Gregory, P. Classification of Dyes by Chemical Structure. In *The Chemistry and Application of Dyes*; David, R., Waring, G.H., Eds.; Springer: New York, NY, USA, 2012; pp. 1–414, ISBN 978-1-4684-7717-7.
10. Ardila-Leal, L.D.; Poutou-Piñales, R.A.; Pedroza-Rodríguez, A.M.; Quevedo-Hidalgo, B.E.; Capela, I.; Kamali, M.; Zuorro, A. A Brief History of Colour, the Environmental Impact of Synthetic Dyes and Removal by Using Laccases. *Molecules* **2021**, *26*, 3813. [[CrossRef](#)]
11. Mo, J.H.; Lee, Y.H.; Kim, J.; Jeong, J.Y.; Jegal, J. Treatment of dye aqueous solutions using nanofiltration polyamide composite membranes for the dye wastewater reuse. *Dye. Pigment.* **2008**, *76*, 429–434. [[CrossRef](#)]

12. Shabbir, S.; Faheem, M.; Ali, N.; Kerr, P.G.; Wu, Y. Periphyton biofilms: A novel and natural biological system for the effective removal of sulphonated azo dye methyl orange by synergistic mechanism. *Chemosphere* **2017**, *167*, 236–246. [[CrossRef](#)]
13. Alex Mbachu, C.; Kamoru Babayemi, A.; Chinedu Egbosuba, T.; Ifeanyichukwu Ike, J.; Jacinta Ani, I.; Mustapha, S. Green synthesis of iron oxide nanoparticles by Taguchi design of experiment method for effective adsorption of methylene blue and methyl orange from textile wastewater. *Results Eng.* **2023**, *19*, 101198. [[CrossRef](#)]
14. Zhu, Y.; Ma, L.; Hai, X.; Yang, Z.; Li, X.; Chen, M.; Yuan, M.; Xiong, H.; Gao, Y.; Wang, L.; et al. Adsorption of methyl orange by porous membranes prepared from deep eutectic supramolecular polymer-modified chitosan. *Environ. Res.* **2023**, *236*, 116778. [[CrossRef](#)]
15. Yang, D.; Qiu, L.; Yang, Y. Efficient Adsorption of Methyl Orange Using a Modified Chitosan Magnetic Composite Adsorbent. *J. Chem. Eng. Data* **2016**, *61*, 3933–3940. [[CrossRef](#)]
16. Liu, S.; Bu, Y.; Cheng, S.; Tao, Y.; Hong, W. Preparation of g-C<sub>3</sub>N<sub>5</sub>/g-C<sub>3</sub>N<sub>4</sub> heterojunction for methyl orange photocatalytic degradation: Mechanism analysis. *J. Water Process Eng.* **2023**, *54*, 104019. [[CrossRef](#)]
17. Igwegbe, C.A.; Onukwuli, O.D.; Ighalo, J.O.; Umembamalu, C.J. Electrocoagulation-flocculation of aquaculture effluent using hybrid iron and aluminium electrodes: A comparative study. *Chem. Eng. J. Adv.* **2021**, *6*, 100107. [[CrossRef](#)]
18. Aysan, H.; Edebalı, S.; Ozdemir, C.; Celik Karakaya, M.; Karakaya, N. Use of chabazite, a naturally abundant zeolite, for the investigation of the adsorption kinetics and mechanism of methylene blue dye. *Microporous Mesoporous Mater.* **2016**, *235*, 78–86. [[CrossRef](#)]
19. Abdul Mubarak, N.S.; Chuan, T.W.; Khor, H.P.; Jawad, A.H.; Wilson, L.D.; Sabar, S. Immobilized Fe-Loaded Chitosan Film for Methyl Orange Dye Removal: Competitive Ions, Reusability, and Mechanism. *J. Polym. Environ.* **2021**, *29*, 1050–1062. [[CrossRef](#)]
20. Madhav, S.; Ahamad, A.; Singh, P.; Mishra, P.K. A review of textile industry: Wet processing, environmental impacts, and effluent treatment methods. *Environ. Qual. Manag.* **2018**, *27*, 31–41. [[CrossRef](#)]
21. Iwuozor, K.O.; Ighalo, J.O.; Emenike, E.C.; Ogunfowora, L.A.; Igwegbe, C.A. Adsorption of methyl orange: A review on adsorbent performance. *Curr. Res. Green Sustain. Chem.* **2021**, *4*, 100179. [[CrossRef](#)]
22. Heidarinejad, Z.; Dehghani, M.H.; Heidari, M.; Javedan, G.; Ali, I.; Sillanpää, M. Methods for preparation and activation of activated carbon: A review. *Environ. Chem. Lett.* **2020**, *18*, 393–415. [[CrossRef](#)]
23. Diaz-Uribe, C.; Angulo, B.; Patiño, K.; Hernández, V.; Vallejo, W.; Gallego-Cartagena, E.; Romero Bohórquez, A.R.; Zarate, X.; Schott, E. Cyanobacterial Biomass as a Potential Biosorbent for the Removal of Recalcitrant Dyes from Water. *Water* **2021**, *13*, 3176. [[CrossRef](#)]
24. Hosny, N.M.; Goma, I.; Elmahgary, M.G. Adsorption of polluted dyes from water by transition metal oxides: A review. *Appl. Surf. Sci. Adv.* **2023**, *15*, 100395. [[CrossRef](#)]
25. Afifah, N.; Adriani, S.; Djaja, N.F.; Saleh, R. Photocatalytic Degradation of Methylene Blue and Methyl Orange with Fe-Doped ZnO Nanoparticles Modified with Natural Zeolite and Montmorillonite: Comparative Study. *Adv. Mater. Res.* **2015**, *1123*, 295–302. [[CrossRef](#)]
26. Dehghani, M.H.; Tajik, S.; Panahi, A.; Khezri, M.; Zarei, A.; Heidarinejad, Z.; Yousefi, M. Adsorptive removal of noxious cadmium from aqueous solutions using poly urea-formaldehyde: A novel polymer adsorbent. *MethodsX* **2018**, *5*, 1148–1155. [[CrossRef](#)]
27. Rex, P.; Rahiman, K.; Ismail, M.; Meenakshisundaram, N.; Barmavatu, P.; Sai Bharadwaj, S.L. Agricultural Biomass Waste to Biochar: A Review on Biochar Applications Using Machine Learning Approach and Circular Economy. *ChemEngineering* **2023**, *7*, 50. [[CrossRef](#)]
28. Johannes Lehmann, S.J. Biochar for environmental management: An introduction. In *Biochar for Environmental Management*; Taylor & Francis: London, UK, 2015; pp. 1–13. ISBN 9780203762264.
29. Praveen, S.; Jegan, J.; Bhagavathi Pushpa, T.; Gokulan, R.; Bulgariu, L. Biochar for removal of dyes in contaminated water: An overview. *Biochar* **2022**, *4*, 10. [[CrossRef](#)]
30. Aborisade, M.A.; Oba, B.T.; Kumar, A.; Liu, J.; Chen, D.; Okimiji, O.P.; Zhao, L. Remediation of metal toxicity and alleviation of toxic metals-induced oxidative stress in *Brassica chinensis* L. using biochar-iron nanocomposites. *Plant Soil* **2023**, 1–17. [[CrossRef](#)]
31. Aborisade, M.A.; Feng, A.; Zheng, X.; Oba, B.T.; Kumar, A.; Battamo, A.Y.; Kavwenje, S.; Liu, J.; Chen, D.; Okimiji, O.P.; et al. Carbothermal reduction synthesis of eggshell-biochar modified with nanoscale zerovalent iron/activated carbon for remediation of soil polluted with lead and cadmium. *Environ. Nanotechnol. Monit. Manag.* **2022**, *18*, 100726. [[CrossRef](#)]
32. Aborisade, M.A.; Geng, H.; Oba, B.T.; Kumar, A.; Ndudi, E.A.; Battamo, A.Y.; Liu, J.; Chen, D.; Okimiji, O.P.; Ojekunle, O.Z.; et al. Remediation of soil polluted with Pb and Cd and alleviation of oxidative stress in *Brassica rapa* plant using nanoscale zerovalent iron supported with coconut-husk biochar. *J. Plant Physiol.* **2023**, *287*, 154023. [[CrossRef](#)]
33. Salzano de Luna, M.; Castaldo, R.; Altobelli, R.; Gioiella, L.; Filippone, G.; Gentile, G.; Ambrogi, V. Chitosan hydrogels embedding hyper-crosslinked polymer particles as reusable broad-spectrum adsorbents for dye removal. *Carbohydr. Polym.* **2017**, *177*, 347–354. [[CrossRef](#)]
34. Munagapati, V.S.; Yarramuthi, V.; Kim, D.S. Methyl orange removal from aqueous solution using goethite, chitosan beads and goethite impregnated with chitosan beads. *J. Mol. Liq.* **2017**, *240*, 329–339. [[CrossRef](#)]
35. Brião, G.V.; Jahn, S.L.; Foletto, E.L.; Dotto, G.L. Highly efficient and reusable mesoporous zeolite synthesized from a biopolymer for cationic dyes adsorption. *Colloids Surf. A Physicochem. Eng. Asp.* **2018**, *556*, 43–50. [[CrossRef](#)]
36. Hammud, H.H.; Shmait, A.; Hourani, N. Removal of Malachite Green from water using hydrothermally carbonized pine needles. *RSC Adv.* **2015**, *5*, 7909–7920. [[CrossRef](#)]

37. Parab, H.; Sudersanan, M.; Shenoy, N.; Pathare, T.; Vaze, B. Use of Agro-Industrial Wastes for Removal of Basic Dyes from Aqueous Solutions. *CLEAN—Soil Air Water* **2009**, *37*, 963–969. [[CrossRef](#)]
38. Mirzaei, D.; Zabardasti, A.; Mansourpanah, Y.; Sadeghi, M.; Farhadi, S. Efficacy of Novel NaX/MgO–TiO<sub>2</sub> Zeolite Nanocomposite for the Adsorption of Methyl Orange (MO) Dye: Isotherm, Kinetic and Thermodynamic Studies. *J. Inorg. Organomet. Polym. Mater.* **2020**, *30*, 2067–2080. [[CrossRef](#)]
39. Lu, K.; Wang, T.; Zhai, L.; Wu, W.; Dong, S.; Gao, S.; Mao, L. Adsorption behavior and mechanism of Fe-Mn binary oxide nanoparticles: Adsorption of methylene blue. *J. Colloid Interface Sci.* **2019**, *539*, 553–562. [[CrossRef](#)]
40. Shah, S.S.; Sharma, T.; Dar, B.A.; Bamezai, R.K. Adsorptive removal of methyl orange dye from aqueous solution using populus leaves: Insights from kinetics, thermodynamics and computational studies. *Environ. Chem. Ecotoxicol.* **2021**, *3*, 172–181. [[CrossRef](#)]
41. Hua, Z.; Pan, Y.; Hong, Q. Adsorption of Congo red dye in water by orange peel biochar modified with CTAB. *RSC Adv.* **2023**, *13*, 12502–12508. [[CrossRef](#)]
42. Ali, S.; Akter, S.; Fogarassy, C.; Rosen, M.A.; Micillo, R.; Alfieri, M.L. Analysis of Circular Thinking in Consumer Purchase Intention to Buy Sustainable Waste-To-Value (WTV) Foods. *Sustainability* **2021**, *13*, 5390. [[CrossRef](#)]
43. McKay, G.; Parthasarathy, P.; Saleem, J.; Alherbawi, M.; Sajjad, S. Dye removal using biochars. *Sustain. Biochar Water Wastewater Treat.* **2022**, 429–471. [[CrossRef](#)]
44. Ramírez-García, R.; Gohil, N.; Singh, V. Recent Advances, Challenges, and Opportunities in Bioremediation of Hazardous Materials. *Phytomanag. Polluted Sites Mark. Oppor. Sustain. Phytoremediat.* **2018**, 517–568. [[CrossRef](#)]
45. Sri Shalini, S.; Palanivelu, K.; Ramachandran, A.; Raghavan, V. Biochar from biomass waste as a renewable carbon material for climate change mitigation in reducing greenhouse gas emissions—A review. *Biomass Convers. Biorefinery* **2020**, *11*, 2247–2267. [[CrossRef](#)]
46. He, M.; Xu, Z.; Hou, D.; Gao, B.; Cao, X.; Ok, Y.S.; Rinklebe, J.; Bolan, N.S.; Tsang, D.C.W. Waste-derived biochar for water pollution control and sustainable development. *Nat. Rev. Earth Environ.* **2022**, *3*, 444–460. [[CrossRef](#)]
47. Seow, Y.X.; Tan, Y.H.; Mubarak, N.M.; Kandedo, J.; Khalid, M.; Ibrahim, M.L.; Ghasemi, M. A review on biochar production from different biomass wastes by recent carbonization technologies and its sustainable applications. *J. Environ. Chem. Eng.* **2022**, *10*, 107017. [[CrossRef](#)]
48. Amalina, F.; Razak, A.S.A.; Krishnan, S.; Sulaiman, H.; Zularisam, A.W.; Nasrullah, M. Biochar production techniques utilizing biomass waste-derived materials and environmental applications—A review. *J. Hazard. Mater. Adv.* **2022**, *7*, 100134. [[CrossRef](#)]
49. Yaashikaa, P.R.; Kumar, P.S.; Varjani, S.; Saravanan, A. A critical review on the biochar production techniques, characterization, stability and applications for circular bioeconomy. *Biotechnol. Rep.* **2020**, *28*, e00570. [[CrossRef](#)] [[PubMed](#)]
50. Sewu, D.D.; Boakye, P.; Woo, S.H. Highly efficient adsorption of cationic dye by biochar produced with Korean cabbage waste. *Bioresour. Technol.* **2017**, *224*, 206–213. [[CrossRef](#)]
51. Nithyalakshmi, B.; Saraswathi, R. Removal of colorants from wastewater using biochar derived from leaf waste. *Biomass Convers. Biorefinery* **2023**, *13*, 1311–1327. [[CrossRef](#)]
52. Abd-Elhamid, A.I.; Emran, M.; El-Sadek, M.H.; El-Shanshory, A.A.; Soliman, H.M.A.; Akl, M.A.; Rashad, M. Enhanced removal of cationic dye by eco-friendly activated biochar derived from rice straw. *Appl. Water Sci.* **2020**, *10*, 45. [[CrossRef](#)]
53. Del Carmen Jaimes, J.M.; Alonso Restrepo, D.; Acevedo, D.C. Preparation and determination of the functional properties of the trupillo proteic concentrated (prosopis juliflora) preparação e determinação das propriedades funcionais nos concentrados de proteínas de trupillo. *Biotechnol. En El Sect. Agropecu. Y Agroind.* **2014**, *12*, 144–152.
54. Muller, G.C.; Junnila, A.; Traore, M.M.; Traore, S.F.; Doumbia, S.; Sissoko, F.; Dembele, S.M.; Schlein, Y.; Arheart, K.L.; Revay, E.E.; et al. The invasive shrub *Prosopis juliflora* enhances the malaria parasite transmission capacity of *Anopheles* mosquitoes: A habitat manipulation experiment. *Malar. J.* **2017**, *16*, 237. [[CrossRef](#)] [[PubMed](#)]
55. Li, J.; Li, Y.; Wu, Y.; Zheng, M. A comparison of biochars from lignin, cellulose and wood as the sorbent to an aromatic pollutant. *J. Hazard. Mater.* **2014**, *280*, 450–457. [[CrossRef](#)] [[PubMed](#)]
56. Diaz-Urbe, C.; Walteros, L.; Duran, F.; Vallejo, W.; Romero Bohórquez, A.R. *Prosopis juliflora* Seed Waste as Biochar for the Removal of Blue Methylene: A Thermodynamic and Kinetic Study. *ACS Omega* **2022**, *7*, 42916–42925. [[CrossRef](#)] [[PubMed](#)]
57. Lewandowski, W.M.; Januszewicz, K.; Kosakowski, W. Efficiency and proportions of waste tyre pyrolysis products depending on the reactor type—A review. *J. Anal. Appl. Pyrolysis* **2019**, *140*, 25–53. [[CrossRef](#)]
58. Cardenas-Peña, A.M.; Ibanez, J.G.; Vasquez-Medrano, R. Determination of the Point of Zero Charge for Electrocoagulation Precipitates from an Iron Anode. *Int. J. Electrochem. Sci.* **2012**, *7*, 6142–6153. [[CrossRef](#)]
59. Hamzenejad Taghliabad, R.; Sepehr, E.; Khodaverdiloo, H.; Samadi, A.; Rasouli-Sadaghiani, M.H. Characterization of cadmium adsorption on two cost-effective biochars for water treatment. *Arab. J. Geosci.* **2020**, *13*, 448. [[CrossRef](#)]
60. Kwak, J.H.; Islam, M.S.; Wang, S.; Messele, S.A.; Naeth, M.A.; El-Din, M.G.; Chang, S.X. Biochar properties and lead(II) adsorption capacity depend on feedstock type, pyrolysis temperature, and steam activation. *Chemosphere* **2019**, *231*, 393–404. [[CrossRef](#)]
61. Geng, Y.; Zhang, J.; Zhou, J.; Lei, J. Study on adsorption of methylene blue by a novel composite material of TiO<sub>2</sub> and alum sludge. *RSC Adv.* **2018**, *8*, 32799. [[CrossRef](#)]
62. Ayawei, N.; Ebelegi, A.N.; Wankasi, D. Modelling and Interpretation of Adsorption Isotherms. *J. Chem.* **2017**, *2017*, 3039817. [[CrossRef](#)]

63. Zou, Y.; Xu, F.; Kong, Q.; Shang, D.; Zhang, Y.; Guo, W.; Wang, Q.; Zhao, C.; Du, Y. Pb<sup>2+</sup> removal performance by cotton-based and magnetic modified cotton-based biochar prepared from agricultural waste biomass. *Desalin. Water Treat.* **2020**, *207*, 246–257. [[CrossRef](#)]
64. Guo, C.; Zou, J.; Yang, J.; Wang, K.; Song, S. Surface characterization of maize-straw-derived biochar and their sorption mechanism for Pb<sup>2+</sup> and methylene blue. *PLoS ONE* **2020**, *15*, e0238105.
65. Bassilakis, R.; Carangelo, R.M.; Wójtowicz, M.A. TG-FTIR analysis of biomass pyrolysis. *Fuel* **2001**, *80*, 1765–1786. [[CrossRef](#)]
66. Reza, M.S.; Ahmed, A.; Caesarendra, W.; Abu Bakar, M.S.; Shams, S.; Saidur, R.; Aslfattahi, N.; Azad, A.K. Acacia Holosericea: An Invasive Species for Bio-char, Bio-oil, and Biogas Production. *Bioengineering* **2019**, *6*, 33. [[CrossRef](#)] [[PubMed](#)]
67. Dlouhá, J.; Suryanegara, L.; Yano, H. The role of cellulose nanofibres in supercritical foaming of polylactic acid and their effect on the foam morphology. *Soft Matter* **2012**, *8*, 8704–8713. [[CrossRef](#)]
68. Aborisade, M.A.; Feng, A.; Oba, B.T.; Kumar, A.; Battamo, A.Y.; Huang, M.; Chen, D.; Yang, Y.; Sun, P.; Zhao, L. Pyrolytic synthesis and performance efficacy comparison of biochar-supported nanoscale zero-valent iron on soil polluted with toxic metals. *Arch. Agron. Soil Sci.* **2023**, *69*, 2249–2266. [[CrossRef](#)]
69. Cyril, N.; George, J.B.; Joseph, L.; Sylas, V.P. Catalytic Degradation of Methyl Orange and Selective Sensing of Mercury Ion in Aqueous Solutions Using Green Synthesized Silver Nanoparticles from the Seeds of Derris trifoliata. *J. Clust. Sci.* **2019**, *30*, 459–468. [[CrossRef](#)]
70. Pawar, A.; Panwar, N.L. A comparative study on morphology, composition, kinetics, thermal behaviour and thermodynamic parameters of Prosopis Juliflora and its biochar derived from vacuum pyrolysis. *Bioresour. Technol. Rep.* **2022**, *18*, 101053. [[CrossRef](#)]
71. Selvarajoo, A.; Oochit, D. Effect of pyrolysis temperature on product yields of palm fibre and its biochar characteristics. *Mater. Sci. Energy Technol.* **2020**, *3*, 575–583. [[CrossRef](#)]
72. Stylianou, M.; Christou, A.; Dalias, P.; Polycarpou, P.; Michael, C.; Agapiou, A.; Papanastasiou, P.; Fatta-Kassinou, D. Physicochemical and structural characterization of biochar derived from the pyrolysis of biosolids, cattle manure and spent coffee grounds. *J. Energy Inst.* **2020**, *93*, 2063–2073. [[CrossRef](#)]
73. Antonangelo, J.A.; Zhang, H.; Sun, X.; Kumar, A. Physicochemical properties and morphology of biochars as affected by feedstock sources and pyrolysis temperatures. *Biochar* **2019**, *1*, 325–336. [[CrossRef](#)]
74. Huo, W.; Zhou, Z.; Chen, X.; Dai, Z.; Yu, G. Study on CO<sub>2</sub> gasification reactivity and physical characteristics of biomass, petroleum coke and coal chars. *Bioresour. Technol.* **2014**, *159*, 143–149. [[CrossRef](#)] [[PubMed](#)]
75. Min, F.; Zhang, M.; Zhang, Y.; Cao, Y.; Pan, W.P. An experimental investigation into the gasification reactivity and structure of agricultural waste chars. *J. Anal. Appl. Pyrolysis* **2011**, *92*, 250–257. [[CrossRef](#)]
76. Wu, L.; Liu, X.; Lv, G.; Zhu, R.; Tian, L.; Liu, M.; Li, Y.; Rao, W.; Liu, T.; Liao, L. Study on the adsorption properties of methyl orange by natural one-dimensional nano-mineral materials with different structures. *Sci. Rep.* **2021**, *11*, 10640. [[CrossRef](#)]
77. Park, J.H.; Ok, Y.S.; Kim, S.H.; Cho, J.S.; Heo, J.S.; Delaune, R.D.; Seo, D.C. Competitive adsorption of heavy metals onto sesame straw biochar in aqueous solutions. *Chemosphere* **2016**, *142*, 77–83. [[CrossRef](#)] [[PubMed](#)]
78. Amouei, A.I.; Amooey, A.A.; Asgharzadeh, F. *Cadmium Removal from Aqueous Solution by Canola Residues: Adsorption Equilibrium and Kinetics*; Iranian Association of Chemical Engineers (IACHE): Tehran, Iran, 2013; Volume 10.
79. Dinh, V.P.; Xuan, T.D.; Hung, N.Q.; Luu, T.T.; Do, T.T.T.; Nguyen, T.D.; Nguyen, V.D.; Anh, T.T.K.; Tran, N.Q. Primary biosorption mechanism of lead (II) and cadmium (II) cations from aqueous solution by pomelo (*Citrus maxima*) fruit peels. *Environ. Sci. Pollut. Res.* **2021**, *28*, 63504–63515. [[CrossRef](#)]
80. Newcombe, G.; Drikas, M. Adsorption of NOM onto activated carbon: Electrostatic and non-electrostatic effects. *Carbon* **1997**, *35*, 1239–1250. [[CrossRef](#)]
81. Doğan, M.; Abak, H.; Alkan, M. Adsorption of methylene blue onto hazelnut shell: Kinetics, mechanism and activation parameters. *J. Hazard. Mater.* **2009**, *164*, 172–181. [[CrossRef](#)]
82. Vasco, A.P.; Betancur, M.V. Kinetic studies for the adsorptive of indigo carmine by abrasive pellets. *Grup Investig. Ambient Univ. Pontif Boliv* **2014**, *8*, 131–139.
83. Wasewar, K.L.; Prasad, B.; Gulipalli, C.S. Batch study, equilibrium and kinetics of adsorption of selenium using rice husk ash (RHA). *J. Eng. Sci. Technol.* **2011**, *6*, 586–605.
84. Kumar, K.V.; Porkodi, K. Mass transfer, kinetics and equilibrium studies for the biosorption of methylene blue using *Paspalum notatum*. *J. Hazard. Mater.* **2007**, *146*, 214–226. [[CrossRef](#)]
85. Wang, J.; Guo, X. Rethinking of the intraparticle diffusion adsorption kinetics model: Interpretation, solving methods and applications. *Chemosphere* **2022**, *309*, 136732. [[CrossRef](#)] [[PubMed](#)]
86. Qiu, Y.; Zheng, Z.; Zhou, Z.; Sheng, G.D. Effectiveness and mechanisms of dye adsorption on a straw-based biochar. *Bioresour. Technol.* **2009**, *100*, 5348–5351. [[CrossRef](#)]
87. Dutta, S.; Gupta, B.; Srivastava, S.K.; Gupta, A.K. Recent advances on the removal of dyes from wastewater using various adsorbents: A critical review. *Mater. Adv.* **2021**, *2*, 4497–4531. [[CrossRef](#)]
88. Tomczyk, A.; Sokołowska, Z.; Boguta, P. Biochar physicochemical properties: Pyrolysis temperature and feedstock kind effects. *Rev. Environ. Sci. Biotechnol.* **2020**, *19*, 191–215. [[CrossRef](#)]
89. Al-Ghouti, M.A.; Da'ana, D.A. Guidelines for the use and interpretation of adsorption isotherm models: A review. *J. Hazard. Mater.* **2020**, *393*, 122383. [[CrossRef](#)] [[PubMed](#)]

90. Erdogan, F.O. Freundlich, langmuir, temkin, dr and harkins-jura isotherm studies on the adsorption of CO<sub>2</sub> on various porous adsorbents. *Int. J. Chem. React. Eng.* **2019**, *17*, 20180134. [[CrossRef](#)]
91. Islam, M.T.; Saenz-Arana, R.; Hernandez, C.; Guinto, T.; Ahsan, M.A.; Bragg, D.T.; Wang, H.; Alvarado-Tenorio, B.; Noveron, J.C. Conversion of waste tire rubber into a high-capacity adsorbent for the removal of methylene blue, methyl orange, and tetracycline from water. *J. Environ. Chem. Eng.* **2018**, *6*, 3070–3082. [[CrossRef](#)]
92. Ambaye, T.G.; Vaccari, M.; van Hullebusch, E.D.; Amrane, A.; Rtimi, S. Mechanisms and adsorption capacities of biochar for the removal of organic and inorganic pollutants from industrial wastewater. *Int. J. Environ. Sci. Technol.* **2020**, *18*, 3273–3294. [[CrossRef](#)]
93. Feng, Y.; Zhou, H.; Liu, G.; Qiao, J.; Wang, J.; Lu, H.; Yang, L.; Wu, Y. Methylene blue adsorption onto swede rape straw (*Brassica napus* L.) modified by tartaric acid: Equilibrium, kinetic and adsorption mechanisms. *Bioresour. Technol.* **2012**, *125*, 138–144. [[CrossRef](#)]
94. Brown, R.W.; Chadwick, D.R.; Bott, T.; West, H.M.; Wilson, P.; Hodgins, G.R.; Snape, C.E.; Jones, D.L. Biochar application to temperate grasslands: Challenges and opportunities for delivering multiple ecosystem services. *Biochar* **2023**, *5*, 33. [[CrossRef](#)]
95. Yönten, V.; Sanyürek, N.K.; Kivanç, M.R. A thermodynamic and kinetic approach to adsorption of methyl orange from aqueous solution using a low cost activated carbon prepared from *Vitis vinifera* L. *Surf. Interfaces* **2020**, *20*, 100529. [[CrossRef](#)]
96. Darwish, A.A.A.; Rashad, M.; AL-Aoh, H.A. Methyl orange adsorption comparison on nanoparticles: Isotherm, kinetics, and thermodynamic studies. *Dye. Pigment.* **2019**, *160*, 563–571. [[CrossRef](#)]
97. Chen, H.; Zhao, J.; Wu, J.; Dai, G. Isotherm, thermodynamic, kinetics and adsorption mechanism studies of methyl orange by surfactant modified silkworm exuviae. *J. Hazard. Mater.* **2011**, *192*, 246–254. [[CrossRef](#)] [[PubMed](#)]
98. Khan, A.; Naem, A.; Mahmood, T. Thermodynamic Study of Adsorption of Methyl Orange and Congo Red from Aqueous Solutions by PVP-Functionalized ZnO. *Russ. J. Phys. Chem. A* **2020**, *94*, 1581–1586. [[CrossRef](#)]
99. Gunay Gurer, A.; Aktas, K.; Ozkaleli Akcetin, M.; Erdem Unsar, A.; Asilturk, M. Adsorption Isotherms, Thermodynamics, and Kinetic Modeling of Methylene Blue onto Novel Carbonaceous Adsorbent Derived from Bitter Orange Peels. *Water. Air. Soil Pollut.* **2021**, *232*, 138. [[CrossRef](#)]
100. Mohammadi, N.; Khani, H.; Gupta, V.K.; Amereh, E.; Agarwal, S. Adsorption process of methyl orange dye onto mesoporous carbon material—kinetic and thermodynamic studies. *J. Colloid Interface Sci.* **2011**, *362*, 457–462. [[CrossRef](#)]
101. El Maguana, Y.; Elhadiri, N.; Benchanaa, M.; Chikri, R. Adsorption Thermodynamic and Kinetic Studies of Methyl Orange onto Sugar Scum Powder as a Low-Cost Inorganic Adsorbent. *J. Chem.* **2020**, *2020*, 9165874. [[CrossRef](#)]
102. Yu, J.; Zhang, X.; Wang, D.; Li, P. Adsorption of methyl orange dye onto biochar adsorbent prepared from chicken manure. *Water Sci. Technol.* **2018**, *77*, 1303–1312. [[CrossRef](#)]
103. Wang, B.; Zhu, Y.; Bai, Z.; Luque, R.; Xuan, J. Functionalized chitosan biosorbents with ultra-high performance, mechanical strength and tunable selectivity for heavy metals in wastewater treatment. *Chem. Eng. J.* **2017**, *325*, 350–359. [[CrossRef](#)]

**Disclaimer/Publisher’s Note:** The statements, opinions and data contained in all publications are solely those of the individual author(s) and contributor(s) and not of MDPI and/or the editor(s). MDPI and/or the editor(s) disclaim responsibility for any injury to people or property resulting from any ideas, methods, instructions or products referred to in the content.